Bull. Mater. Sci., Vol. 40, No. 5, September 2017, pp. 983–990
DOI 10.1007/s12034-017-1456-3
© Indian Academy of Sciences

Fabrication and enhanced photoluminescence properties of $NaLa(MoO_4)_2$: Sm^{3+}, Bi^{3+} phosphors with high efficiency white-light-emitting

XINGSHUANG ZHANG[1], GUANGJUN ZHOU[1,*], JUAN ZHOU[2], HAIFENG ZHOU[1], PENG KONG[1], ZHICHAO YU[1] and JIE ZHAN[1]

[1]State Key Laboratory of Crystal Materials, Shandong University, Jinan 250100, People's Republic of China
[2]Center for Disease Prevention and Control of Jinan Military Command, Jinan 250014, People's Republic of China
*Author for correspondence (gjzhou@sdu.edu.cn)

MS received 4 March 2016; accepted 5 December 2016; published online 29 August 2017

Abstract. The tetragonal scheelite-type Sm^{3+}/Bi^{3+} ions co-doped with $NaLa(MoO_4)_2$ phosphors were synthesized by a facile sol–gel and combustion process using citric acid as complexing agent. The crystal structure and morphology of these as-prepared samples were characterized by X-ray diffraction (XRD) and scanning electron microscopy (SEM). Furthermore, UV-absorption and the photoluminescence (PL) properties of these phosphors were systematically investigated and the PL of the phosphors shows strong white light emissions. Efficient energy transfer from the MoO_4^{2-} group or Bi^{3+} ions to Sm^{3+} ions was established by PL investigation excited at 405 nm. The PL intensity of the studied materials was investigated as a function of different Sm^{3+} and Bi^{3+} concentrations. The PL investigations revealed that the phosphors exhibit apparent characteristic emissions, which is ascribed to the transition from the ground state energy level $^4G_{5/2}$ to excited state energy levels ^6H_J ($J = 5/2, 7/2, 9/2$) and the $NaLa(MoO_4)_2$: 4 mol% Sm^{3+} and $NaLa(MoO_4)_2$: 4 mol% Sm^{3+}, 8 mol% Bi^{3+} present white emissions with the CIE coordinates of (0.350, 0.285) and (0.285, 0.229), respectively. The absolute quantum efficiencies of the phosphors are 40% ($NaLa(MoO_4)_2$: 4 mol% Sm^{3+}) and 52% ($NaLa(MoO_4)_2$: 4 mol% Sm^{3+}, 8 mol% Bi^{3+}), respectively.

Keywords. Optical properties; sol–gel processes; combustion method; photoluminescence.

1. Introduction

Over the past several decades, the rare earth ions doped with double alkaline molybdate compounds have been extensively studied in the fields of phosphors, laser, scintillation counters, optical fibres and biolabels due to their excellent luminescent properties and chemical stability [1–7]. In fact, molybdates present high monochromaticity, long life-time, high energy efficiency and high resistance to photobleaching and they have been proven to be excellent host materials for photoactive lanthanide ions [8]. The previous studies for $ALn(MO_4)_2$(A^+= alkali metal ions; Ln^{3+}= trivalent rare earth ions; M = Mo, W) family compounds mainly focused on the single crystals, which could be used as laser crystal materials [9,10].

Up to now, there has been an increasing trend towards the designable and controllable synthesis of micro/nano materials with regular morphologies, such as microflowers, dendritic, ellipsoid, micro-spheres, microrugbies, thin plates, quasi-cubes, shuttle-like and urchin-like architectures, etc. [11–17]. In particular, as host materials for Ln^{3+} ions doping, the $NaLa(MoO_4)_2$ type materials generally exhibit fine luminescence properties, which may be widely applied in solid state lightings as light conversion phosphors [18]. Generally, $NaLa(MoO_4)_2$ possesses a scheelite-like ($CaMoO_4$) structure. There are various approaches to synthesize the rare earth molybdate nanocrystals and sub-microcrystals, such as combustion synthesis [19], co-precipitation method [20], solid state reaction [21], hydrothermal process [22], molten salt synthesis [23], sol–gel synthesis [24,25] and microemulsion method [26]. The synthesis, structures, morphologies, down/up conversion luminescence of $NaCe(MoO_4)_2$ [11], $NaLa(MoO_4)_2$ [12], $NaGd(MoO_4)_2$: Ln^{3+}(Ln = Eu, Tb, Dy and Sm) [3], $NaEu(MoO_4)_2$ [14], $NaY(MoO_4)_2$ [27,28], $BaGd_2(MoO_4)_4$: Ln^{3+} (Ln = Sm, Er and Dy) [21] have been studied. Many phosphors have been applied on white LED, such as a yellow emitting phosphor $Y_3Al_5O_{12}$: Ce^{3+}, YAG: Ce^{3+} based on blue InGaN LED [29]. It is necessary to add a red component to enhance the colour rendering index. Therefore, researches on high efficiency red phosphors are very important. So far, lanthanide ions doped sulphide and nitride red phosphors, for example, Y_2O_2S: Eu^{3+}, $SrGa_2S_4$: Eu^{2+}, $Sr_3Si_5N_8$: Eu^{2+} and $CaSiAlN_3$: Eu^{2+} are widely being used for solid-state lightings [30,31]. Kasturi [32] reports a novel red line emitting phosphors for pcLEDs, $La_2W_{2-x}Mo_xO_9$: Eu^{3+} and analyses their Judd-Ofelt. RE ions doped with luminescent materials generally have fascinating

optical characteristics because of their unique intra-4f transition, leading to a sharp emission and narrow band. In addition, they hardly depend on the co-ordination environment or crystal field owing to the shielding of the 4f orbits by the 5s and 5p orbits. The intense orange light emission of Sm^{3+} activated different inorganic phosphors. Host materials are very useful in the fabrication of white-light-emitting diodes by taking the combination of UV-LED with cyan and orange emitting phosphor materials [33]. In many reports, it can be found that the doping of Bi^{3+} in some host materials could enhance the PL intensity of these phosphors and Bi^{3+} can be explored as either an activator or a sensitizer in some host materials [34–36]. In our previous work, the co-doping of Ho^{3+}/Bi^{3+} in $LaNbTiO_6$ had been studied and the incorporation of Bi^{3+} enhanced the PL intensity of the phosphors [37]. Many Sm^{3+} singly doped molybdate materials have been studied widely, while Sm^{3+}/Bi^{3+} co-doped with double alkaline molybdate phosphors have not been reported.

Herein, high efficient white-light-emitting $NaLa(MoO_4)_2$ phosphors have been synthesized successfully by sol–gel and combustion process and $NaLa(MoO_4)_2$ had been confirmed to be a fascinating host material for RE ions. In addition, the luminescence properties of RE ions doped with $NaLa(MoO_4)_2$ materials were investigated in detail by varying the molar ratios of Sm^{3+}/Bi^{3+} and calcined temperatures. The obtained phosphors present white-light-emitting and the absolute quantum efficiency of $NaLa(MoO_4)_2$: 4 mol% Sm^{3+}, 8 mol% Bi^{3+} is up to 52%.

2. Materials and methods

2.1 *Experimental*

All the reagents were analytically graded and used as purchased without further purification. Pure and doped $NaLa(MoO_4)_2$ samples were synthesized by using a facile sol–gel and combustion process. Sodium nitrate, lanthanum oxide, hexa-ammonium molybdate, samarium oxide, bismuth nitrate, nitric acid and citric acid were used as starting materials to prepare the phosphor samples. Lanthanum nitrate and samarium nitrate solutions were produced earlier by dissolving the lanthanum oxide and samarium oxide with excess diluted nitric acid, respectively. The acquired lanthanum nitrate and samarium nitrate solutions were heated at 100°C to evaporate water and the excess nitric acid. Then, the lanthanum nitrate, samarium nitrate and bismuth nitrate were made upto solutions of 0.5, 0.05 and 0.05 mol l^{-1}, respectively. Citric acid was used as a prominent complexant for the sol process, which also facilitated the formation of gel.

In a typical procedure, 2 mmol of sodium nitrate was dissolved in 5 ml deionized water. Then, 4 ml of lanthanum nitrate aqueous solution (0.5 M) was added into sodium nitrate solution. Finally, 6 mmol of citric acid and 0.7062 g of hexa-ammonium molybdate were added into the mixed solution under continuous magnetic stirring at 85°C. After the water evaporated, the transparent sol turned into gel with high viscosity. The gel was dried at 100°C for 24 h to form light yellowish toast bread-like xerogel. The as-obtained xerogel was ground into powder and introduced into crucibles, then directly transferred into a muffle furnace for calcining. The xerogels obtained were kept at sintering temperature of 600, 700, 800, 900 and 1000°C for 5 h, respectively. A similar process was employed for doped samples, which are prepared by adding a stoichiometric amount of samarium nitrate aqueous solution (0.05 M) and bismuth nitrate aqueous solution (0.05 M) instead of lanthanum nitrate aqueous solution. The doping concentration of Sm^{3+} varied from 1 to 6 mol% and Bi^{3+} varied from 2 to 14 mol%. Finally, all samples were ground into powder for further characterization.

2.2 *Characterization*

Phase composition, structure and crystallinity of the products were characterized by X-ray powder diffraction patterns (Germany Bruker Axs D8-Avance X-ray diffractometer with graphite monochromatized Cu Kα irradiation ($\lambda = 1.5418$ Å)), over 10–80°C, with scanning rate of 0.04° s^{-1}. Thermal analysis of the powder dried at 100°C for 24 h was carried out from 30 to 1000°C by using thermogravimetry-differential thermal analyser (TG-DTA) (PerkinElmer Corporation, Diamond TG-DTA) at a constant heating rate of 20°C min^{-1}. Microstructure and stoichiometry of the samples were examined by using scanning electron microscopy (SEM) (Hitachi, S-4800). The ultraviolet–visible (UV–Vis) absorption spectra were taken with a Shimadzu UV-2100 spectrometer. The PL property was recorded by using a fluorescence spectrophotometer (JEOL, F-4500 and FLS920) and a 450 W Xe lamp serves as the excitation source. Absolute quantum efficiencies of the phosphor and the decay time of the excited states were measured by an Edinburgh FLS920 fluorescence spectrometer equipped with a quantum yield measurement system. All the measurements were taken at room temperature.

3. Results and discussion

3.1 *Structure and morphology*

The composition and phase purity of the samples were identified by X-ray diffraction (XRD) patterns. The XRD patterns of the as-synthesized pure $NaLa(MoO_4)_2$ samples were calcined at different sintering temperatures (600, 700, 800, 900 and 1000°C) for 5 h, $NaLa(MoO_4)_2$: 4 mol% Sm^{3+} and $NaLa(MoO_4)_2$: 4 mol% Sm^{3+}, 8 mol% Bi^{3+} calcined at 900°C for 5 h are presented in figure 1. From figure 1a, comparing the XRD patterns of the samples with the standard pattern of tetragonal $NaLa(MoO_4)_2$ (JCPDS card 24-1103), all diffraction peaks of the different samples can be well indexed to scheelite-like ($CaMoO_4$) structure $NaLa(MoO_4)_2$ with the tetragonal space group of $I4_1/a(88)$ and the lattice constants were calculated to be $a = b = 5.2323$ Å,

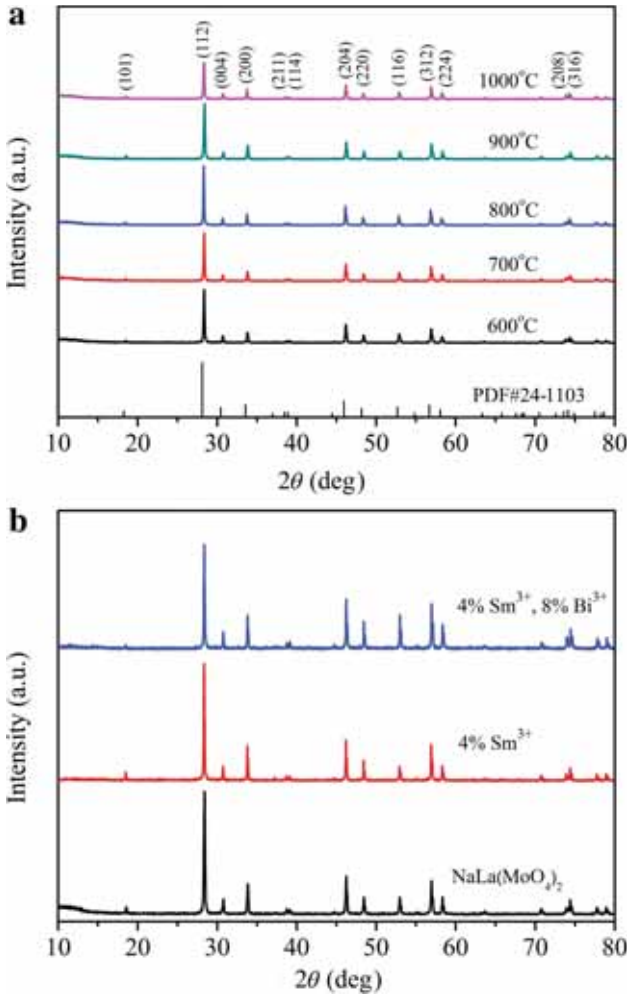

Figure 1. (**a**) XRD patterns of the as-prepared pure $NaLa(MoO_4)_2$ samples calcined at different sintering temperatures (600, 700, 800, 900 and 1000°C) for 5 h. The standard pattern of tetragonal $NaLa(MoO_4)_2$ (JCPDS card 24-1103) is also presented at the bottom for comparison. (**b**) XRD patterns of pure, 4 mol% Sm^{3+}-doped and 4 mol% Sm^{3+}, 8 mol% Bi^{3+} co-doped $NaLa(MoO_4)_2$ samples calcined at 900°C for 5 h.

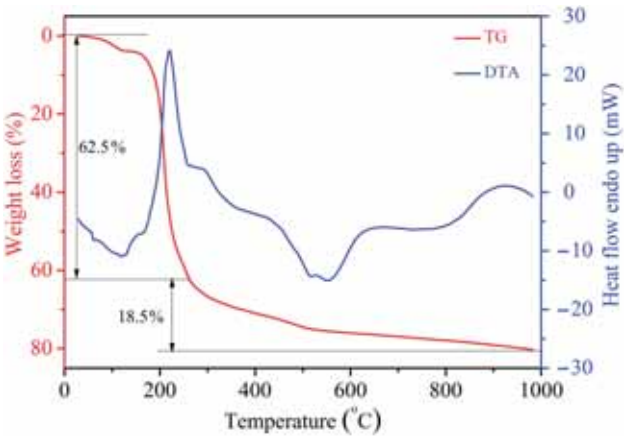

Figure 2. TG–DTA curves of pure $NaLa(MoO_4)_2$ precursor xerogel powder.

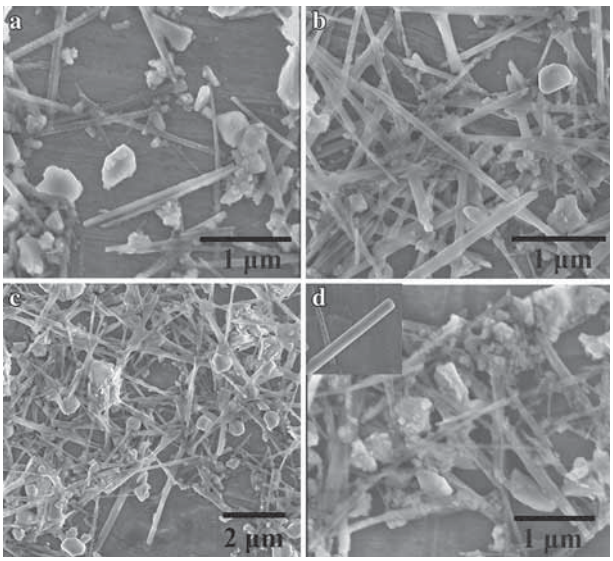

Figure 3. SEM micrographs of pure and doped samples prepared at 900°C for 5 h: (**a**) $NaLa(MoO_4)_2$; (**b**) $NaLa(MoO_4)_2$: 4 mol% Sm^{3+}; (**c**) and (**d**) $NaLa(MoO_4)_2$: 4 mol% Sm^{3+}, 8 mol% Bi^{3+}.

$c = 11.8651$ Å. No additional impurity peak is detected. In the standard pattern, the lattice constants are $a = b = 5.343$ Å, $c = 11.743$ Å. In this structure, Mo^{6+} is co-ordinated by four oxygen atoms in a tetrahedral site while the RE^{3+} ions or alkali metal ions are eight coordinated and located in oxygen polyhedron in the form of REO_8 units with two sets of metal-oxygen distances [38,39]. In addition, the well matched XRD results in figure 1b indicate that Sm^{3+} ions doping and Sm^{3+}/Bi^{3+} co-doping can hardly cause obvious changes to the host structure and phase purity.

Figure 2 shows TG–DTA curves of the $NaLa(MoO_4)_2$ xerogel powders, which had been dried at 100°C for 24 h. The TG curve displays two main weight loss stages. The first stage of weight loss is below 258°C and at the stage the sample lost approximately 62.5%. At the same time, in the DTA curve, there is a strong exothermic peak at about 220°C, which can be well explained by the heat generated in combustion of citric acid. At the second stage, the weight loss is about 18.5%, while the temperature rises from 258 to 1000°C. Moreover, there are several weak exothermic peaks, which could be attributed to two reasons: one is the further combustion of remaining citric acid and organic residues and the other is the formation of tetragonal phase. When the combustion process comes to an end, weight loss will keep constant and the samples will undergo no more transformations.

In order to discuss the effect of doping ions on the morphology of the $NaLa(MoO_4)_2$ microcrystals, the scanning electron microscope (SEM) micrographs of the pure and doped samples prepared at 900°C for 5 h are shown in figure 3. From an

overall perspective, all these three samples show solid rod-like morphology in figure 3a–d and the diameter of these rods is about 50–200 nm. Therefore, the doping of Sm^{3+} and Sm^{3+}/Bi^{3+} hardly changes the morphology of the phosphors. As to the pure $NaLa(MoO_4)_2$, the proportion of rods is lower than that in $NaLa(MoO_4)_2$: 4 mol% Sm^{3+}; and (c) $NaLa(MoO_4)_2$: 4 mol% Sm^{3+}, 8 mol% Bi^{3+}. In addition, from figure 3a–d, it can be seen that there are some blocks and irregular particles exist among the rods sintered at high temperature, which can be ascribed to the agglomeration phenomenon in both pure and doped samples.

3.2 *Photoluminescence properties*

Figure 4 shows the UV–Vis absorption spectrum of pure samples calcined at 900°C for 5 h. From figure 4, it can be seen that $NaLa(MoO_4)_2$ has an absorbance with a steep edge in the ultraviolet region. According to the photon energy $E = h\nu$ and $c = \nu\lambda$, the band gap (E_g) can be calculated $E_g = 1240/\lambda_g$ (λ_g is absorption wavelength threshold). λ_g could be obtained through the absorption edge of the sample. From the linear extrapolation in figure 4, the value of E_g was calculated to be 4.46 eV. This suggests that the valence band maximum and conduction band minimum are mainly composed of O2p and Mo4d bands, respectively. The bands attributed to Na/La lie lower in energy than the O2p valence band. This feature in the electronic structure of $NaLa(MoO_4)_2$ leads to a constant value of E_g with stacking faults in RE ions doped with $NaLa(MoO_4)_2$. The obvious absorption in the ultraviolet region is mainly attributed to the charge transfer state (CTS) transition from O^{2-} ligand to Mo^{6+} in MoO_4^{2-} groups.

Figure 5 shows the photoluminescence excitation (PLE) spectrum and the dependence of the Sm^{3+}-doping concentration (x) of the $NaLa(MoO_4)_2 : x\ Sm^{3+}$ ($x = 1-6$ mol%) phosphors calcined at 900°C for 5h on the relative photoluminescence (PL) intensity. As can be seen in figure 5a, the

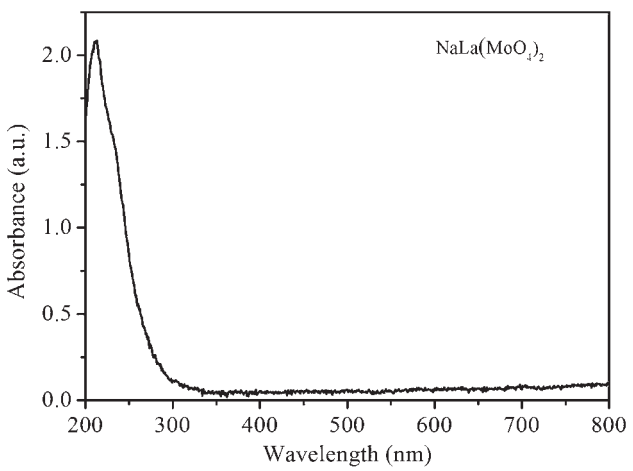

Figure 4. UV–Vis absorption spectra of $NaLa(MoO_4)_2$ samples calcined at 900°C for 5 h.

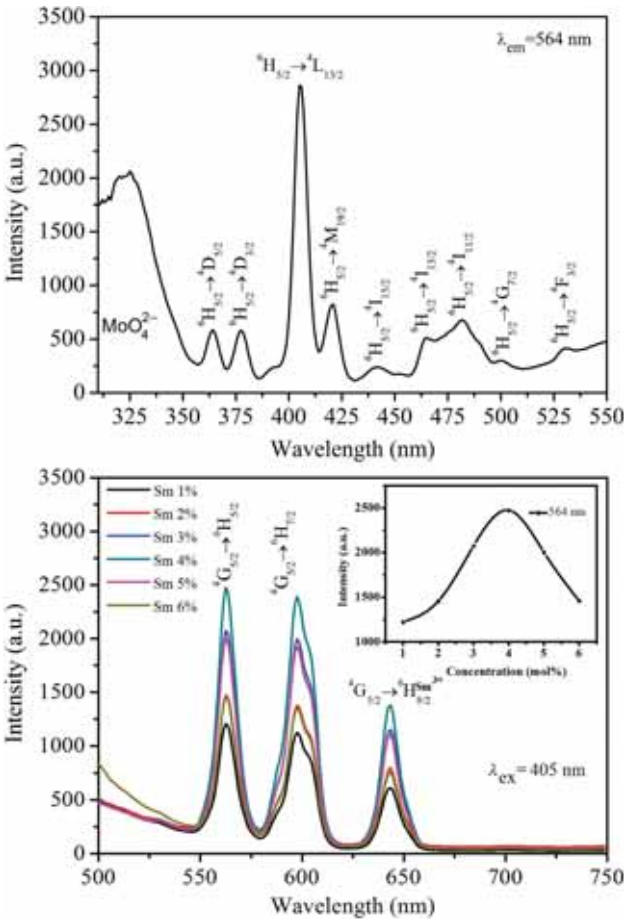

Figure 5. (**a**) Excitation spectrum of Sm^{3+}-doped $NaLa(MoO_4)_2$ sample ($\lambda_{em} = 564$ nm) and (**b**) emission spectra of Sm^{3+}-doped $NaLa(MoO_4)_2$ samples prepared with various doping concentrations ($\lambda_{ex} = 405$ nm). The inset of **b** shows the evolution of the emission intensities at 597 nm as a function of the Sm^{3+} doping concentrations.

excitation spectrum consists of a series of peaks in the range of 310–550 nm, including one strongest peak around 405 nm, a broad band situated at the 200–350 nm region and several sharp peaks intersperse among 350–550 nm. The broad band in the range of 200–350 nm can be ascribed to the host absorption of MoO_4^{2-} involving the CTS of $O^{2-} \rightarrow Mo^{6+}$ [38,39]. As shown in figure 5a, the sharp peaks in the longer wavelength region between 350 and 550 nm are ascribed to intra-configurational 4f–4f transitions from the $^6H_{5/2}$ ground state to the excited state of Sm^{3+}in the host lattice, including 364 nm ($^6H_{5/2} \rightarrow {}^4D_{5/2}$), 377 nm ($^6H_{5/2} \rightarrow {}^4D_{3/2}$), 405 nm ($^6H_{5/2} \rightarrow {}^4L_{13/2}$), 421 nm ($^6H_{5/2} \rightarrow {}^4M_{19/2}$), 441 nm ($^6H_{5/2} \rightarrow {}^4I_{15/2}$), 465 nm ($^6H_{5/2} \rightarrow {}^4I_{13/2}$), 482 nm ($^6H_{5/2} \rightarrow {}^4I_{11/2}$), 500 nm ($^6H_{5/2} \rightarrow {}^4G_{7/2}$) and 530 nm ($^6H_{5/2} \rightarrow {}^4F_{3/2}$), respectively.

At the same time, figure 5b shows the emission spectra of Sm^{3+} doped samples excited at 405 nm. The main three emission peaks originated from the intra-4f shell transitions from the excited energy level $^4G_{5/2}$ to the ground energy ^6H_J

levels ($J = 5/2$, 7/2, 9/2) and they are located at 564 nm ($^4G_{5/2} \rightarrow {}^6H_{5/2}$), 600 nm ($^4G_{5/2} \rightarrow {}^6H_{7/2}$) and 645 nm ($^4G_{5/2} \rightarrow {}^6H_{9/2}$), respectively. The emission intensity of the transitions between energy levels of different J values is related to the point group symmetry of the environment of Sm^{3+} and it is known that the emission band located at 550–600 nm is partially magnetic dipole natured and partially electric dipole allowed transition. According to Judd–Ofelt theory, magnetic dipole transitions obey the selection rule of $|\Delta J| = 0$ and 1, which is insensitive to the environment and the intensity does not change with the matrix [40–42]. In detail, the transition responsible for the orange emission at 564 nm ($^4G_{5/2} \rightarrow {}^6H_{5/2}$) ($|\Delta J| = 0$) has a predominant magnetic dipole character. For the yellow emission at 600 nm the transition from $^4G_{5/2}$ to $^6H_{7/2}$ ($|\Delta J| = 1$) partially belongs to the magnetic dipole transition. Relatively, transition from $^4G_{5/2}$ to $^6H_{9/2}$ ($|\Delta J| = 2$) corresponding to the red emission at 645 nm is the typical electric dipole transition, the intensity of which increases with the reducing of environment symmetry of Sm^{3+} ions. Moreover, the emission ratio of $I(^4G_{5/2} \rightarrow {}^6H_{9/2})/I(^4G_{5/2} \rightarrow {}^6H_{5/2})$ can be used as a measure of the site symmetry and the polarizability of the chemical environment of the Sm^{3+} ions [43]. When the ratio is higher, the symmetry is lower. Figure5b shows that the emission intensity centred at 564 nm is stronger than that at 645 nm, indicating that the magnetic dipole transition is dominant and Sm^{3+} ions hold a higher symmetry site in the host lattice. In addition, the inset of figure 5b presents the evolution of the emission intensity of about 564 nm as a function of Sm^{3+} doping concentration. Initially, the emission intensity increases along with the increase in Sm^{3+} doping concentration; once Sm^{3+} doping concentration increases to a certain level, the PL intensity decreases with the increase in doping concentration due to the concentration quenching effect. That is to say, beyond the optimal concentration of Sm^{3+}(4 mol%), one can expect concentration quenching. Generally, concentration quenching can be caused by energy migration between the same ions (Sm^{3+}) to the killer sites (crystalline defects) [44]. With the concentration of Sm^{3+} ions increasing, the distance between Sm^{3+} ions becomes small enough to allow resonant energy transfer among adjacent Sm^{3+} ions, triggering energy migration to crystalline defects. To understand the energy transfer and concentration quenching processes, the critical distance R_c between adjacent Sm^{3+} ions can be calculated using Eq. (1), as given by Blasse [45,46]:

$$R_c \approx 2\left[\frac{3V}{4\pi X_c Z}\right]^{1/3}, \quad (1)$$

where X_c is the critical concentration, Z is the number of host cations (Na/La^{3+}) per unit cell and V is the volume of the unit cell. In this case, $V = 335.24$ Å^3, $Z = 2$ and $X_c = 0.04$. Using Eq. (1), the critical distance $R_c = 2.00$ nm. When the distance between adjacent Sm^{3+} ions was smaller than this value ($R_{Sm\rightarrow Sm} < R_c$), energy transfer among Sm^{3+} ions dominated. In addition, a theoretical description was developed for the doping concentration *vs*. the luminescence intensity [47]. According to the following Eq. (2) [32]:

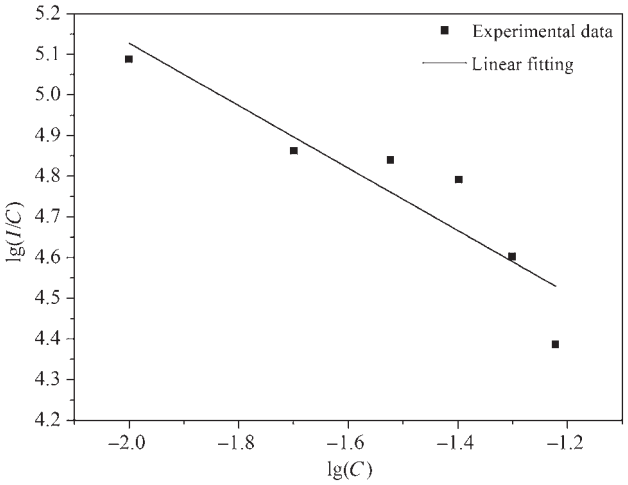

Figure 6. The relationship between the doping concentration (Sm^{3+}) lg(C) and log(I/C) for the $^4G_{5/2} \rightarrow {}^6H_{5/2}$ transition in $NaLa(MoO_4)_2$.

$$\lg\frac{I}{C} = -\frac{s}{d}\lg C + \lg f \quad (2)$$

where I is the luminescence intensity, C is the doping concentration, s is the index of electric multipole, d is a dimension of the sample, here $d = 3$, f is independent of the doping concentration. Figure 6 shows the lg(I/C) *vs*. lg(C) plot for the $NaLa(MoO_4)_2$: Sm^{3+} phosphors. After fitting the line, the slope parameter –s/d was calculated to be –0.77, which is close to 1 (corresponding to $s = 3$), indicating that the energy transfer among Sm^{3+} ions occurs in the phosphor through a dominant exchange interaction mechanism [32].

The PL properties of Sm^{3+} and Bi^{3+} co-doped with $NaLa(MoO_4)_2$ compounds were investigated by varying the concentration of Bi^{3+} ions from 2 to 14 mol% while maintaining the Sm^{3+} concentration at 4 mol%. Figure 7 shows the emission spectra of Sm^{3+}/Bi^{3+} ions co-doped with $NaLa(MoO_4)_2$ phosphors calcined at 900°C for 5 h. At ambient temperature, $NaLa(MoO_4)_2$: 4 mol% Sm^{3+}, yBi^{3+} ($y = 2-14$ mol%) excited at 405 nm present similar emission spectra with Sm^{3+} singly doped sample. However, the PL emission intensity enhanced with the increasing of Bi^{3+} doping concentration and reached a maximum at $y = 8$ mol%. A further increasing of Bi^{3+} resulted in concentration quenching as shown in the inset of figure 7. Herein, the strong CTS of host MoO_4^{2-} group is favourable for the effective energy transfer and luminescence of Sm^{3+}. According to the previous reports, the Bi^{3+} singly doped sample usually exhibits a

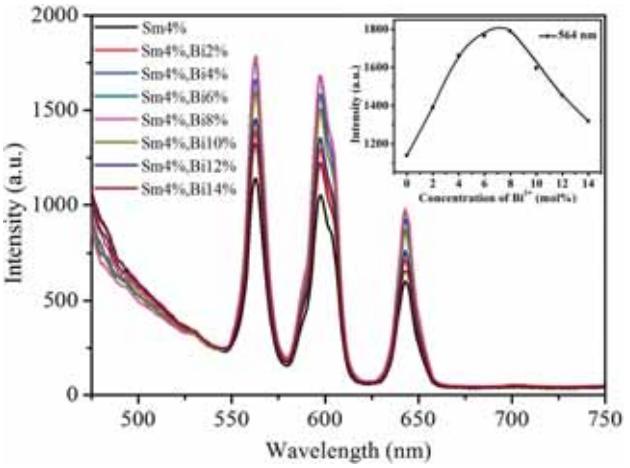

Figure 7. Emission spectra of the Sm^{3+}/Bi^{3+} co-doped $NaLa(MoO_4)_2$ samples with various concentrations of Bi^{3+} excited at 405 nm. The inset shows the evolution of the emission intensities at 564 nm as a function of Bi^{3+} doping concentrations.

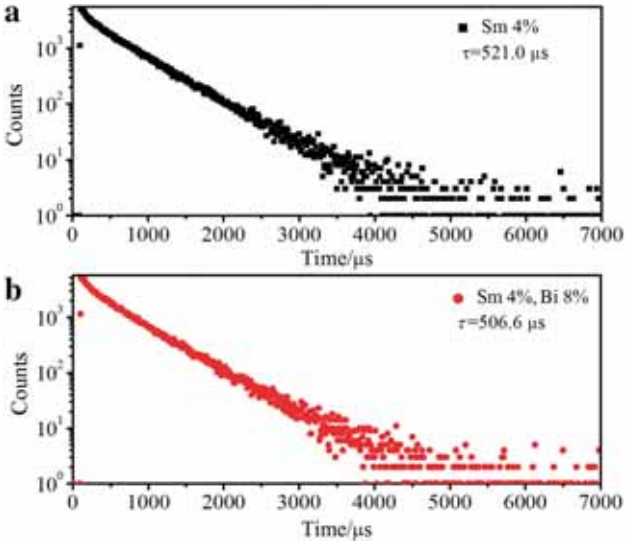

Figure 8. Luminescence decay traces at $^6H_{5/2}$ of Sm^{3+} singly doped and Sm^{3+}/Bi^{3+}co-doped $NaLa(MoO_4)_2$ phosphors monitored at 564 nm ($\lambda_{ex} = 405$ nm).

broad band of purple–blue emission, which extends from 350 to 500 nm when excited by 335 nm. As the self-absorption of Bi^{3+} from ground state $^1S_0$ to excited state $^3P_1$ is overlapped with CTS absorption of host MoO_4^{2-}; the introduction of Bi^{3+} gives rise to absorption of 310–350 nm [35,48,49]. On one hand, according to Kimani *et al* [34], it can be explained that due to the metal–metal charge transfer in which the electrons are transferred from the ns^2 orbital of Bi^{3+} to the nd^0 orbital of Mo^{6+}, the $6s^2-6s6p$ excitations of Bi^{3+} can effectively extend the absorption band closer to the UV light region, resulting in the increase of PL intensity. On the other hand, the Bi^{3+} ion can also be used as a sensitizer due to the efficient energy transfer from Bi^{3+} to Ln^{3+}.

Fluorescence lifetime is the average duration of single excited state of molecules. The fluorescence lifetime of a fluorescent material depends on not only its structure, but also the micro-environment conditions, including polarity, viscosity and so on. Figure 8 exhibits the $Sm^{3+6}H_{5/2}$ energy level decay curves of $NaLa(MoO_4)_2$: 4 mol% Sm^{3+} and $NaLa(MoO_4)_2$: 4 mol% Sm^{3+}, 8 mol% Bi^{3+} phosphors monitored at 564 nm through exciting $^4G_{5/2}$ energy level under 405 nm, where the *Y*-axis was normalized and natural logarithm is taken. The fluorescence lifetimes of Sm^{3+} doped and Sm^{3+}/Bi^{3+} co-doped $NaLa(MoO_4)_2$ samples are 521.0 and 506.6 μs, respectively. Apparently, their lifetimes are very close. According to the excited lifetime theory, fluorescence lifetime is mainly determined by spontaneous radiative transition lifetime and non-radiative transition lifetime. Any processes that compete with spontaneous emission will decrease excited lifetime. On one hand, the introduction of Bi^{3+} could change the symmetry of the crystal field, increase the collision probability and make the system lose some electronic excitation energy, which is complete with spontaneous emission, leading to fluorescence lifetime decrease. On the other hand, the increase of PL intensity of Sm^{3+}/Bi^{3+} co-doped with $NaLa(MoO_4)_2$

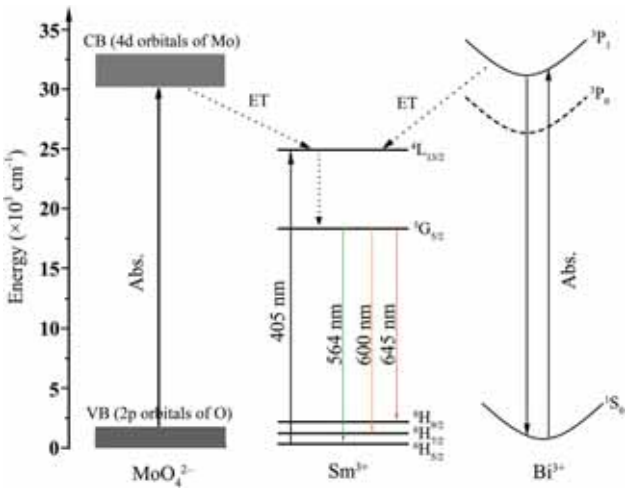

Figure 9. Schematic energy level diagram of the luminescence mechanism of $NaLa(MoO_4)_2 : Sm^{3+}, Bi^{3+}$ phosphors (ET: energy transfer).

samples than Sm^{3+} doped $NaLa(MoO_4)_2$ samples means that the radiative transition probability increases. The introduction of Bi^{3+} in Sm^{3+} doped $NaLa(MoO_4)_2$ samples could increase the radiation transition probability owing to the efficient energy transfer from Bi^{3+} to Sm^{3+}.

As can be seen in figure 9, upon excitation at 405 nm, energy is absorbed by the host leading to the charge transfer of $O^{2-}\rightarrow Mo^{6+}$ and this energy is further transferred to 4f shell of Sm^{3+}. The electrons of Sm^{3+} at $^4G_{5/2}$ excited state can populate both from the non-radiative charge transfer feeding and non-radiative transition from higher excited states $^4L_{13/2}$. Then, the energy could be transferred from $^4G_{5/2}$ to ^6H_J ($J = 5/2, 7/2, 9/2$) energy levels. As an alternative

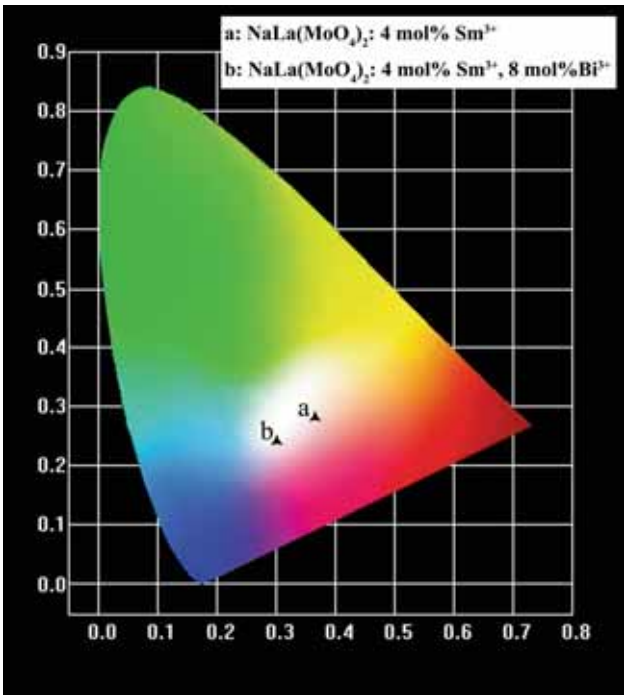

Figure 10. CIE chromaticity diagram for (a) $NaLa(MoO_4)_2$: 4 mol% Sm^{3+} and (b) $NaLa(MoO_4)_2$: 4 mol% Sm^{3+}, 8 mol% Bi^{3+} phosphors ($\lambda_{ex} = 405$ nm).

path of the emission process in $NaLa(MoO_4)_2$ co-doped with Sm^{3+} and Bi^{3+}, the 405 nm exciting energy is either absorbed by Bi^{3+} ion and moves to the excited state energy level $^3P_1$, or transferred to $^4L_{13/2}$ of Sm^{3+} through the non-radiative transition. Finally, $^4G_{5/2}$ energy level of Sm^{3+} relaxes to ^6H_J ($J = 5/2$, 7/2, 9/2) energy levels through electron transition processes, leading to the enhancement of the efficiency of the energy transfer in Sm^{3+} and increase in the PL intensity of the phosphors.

Chromaticity coordinate is one of the vital factors for evaluating performance of the synthesized phosphors. Here, we investigated the luminescent colour of the as-prepared samples by using the Commission Internationale deI' Eclairage (CIE) 1931 diagram. The chromaticity coordinates are calculated based on the emission spectra of $NaLa(MoO_4)_2$: 4 mol% Sm^{3+} and $NaLa(MoO_4)_2$: 4 mol% Sm^{3+}, 8 mol% Bi^{3+}phosphors and they are intuitively presented in the CIE 1931 diagram in figure 10. The CIE chromaticity coordinates of $NaLa(MoO_4)_2$: 4 mol% Sm^{3+} and $NaLa(MoO_4)_2$: 4 mol% Sm^{3+}, 8 mol% Bi^{3+} are (0.350, 0.285) and (0.285, 0.229), respectively, both located in the white region. The absolute fluorescence quantum efficiencies of the phosphors are 40% ($NaLa(MoO_4)_2$: 4 mol% Sm^{3+}) and 52% ($NaLa(MoO_4)_2$: 4 mol% Sm^{3+}, 8 mol% Bi^{3+}). On one hand, quantum efficiency is defined as the ratio between the numbers of emitted protons and incident photons of the sample during the excitation process [50]. On the other hand, the excitation energy absorbed by the phosphor is ideally released in radiative and non-radiative transitions and the fluorescence efficiency might be expressed as the ratio of radiative on radiative plus non-radiative transitions. Transition probability is related to fluorescence quantum efficiency. Before saturable absorption, the greater the transition probability, the stronger was the PL intensity upon the same excitation light. The doping of Bi^{3+} increases the radiative transition probability. Thus, the phosphors co-doped with Sm^{3+}/Bi^{3+} presented stronger PL intensity and fluorescence quantum efficiency compared with samples that singly doped with Sm^{3+}.

4. Conclusions

In summary, a facile sol–gel combustion process has been used to successfully synthesize tetragonal scheelite-type $NaLa(MoO_4)_2$: Sm^{3+}/Bi^{3+} phosphors. The influence of calcined temperature on the crystallinity and the PL intensity of the products were investigated in detail. $NaLa(MoO_4)_2$: Sm^{3+} phosphors present excellent white-light-emitting, whereas the co-doping of Bi^{3+} enhanced the PL intensity of $NaLa(MoO_4)_2$:Sm^{3+}. This can be ascribed to the efficient energy transfer from MoO_4^{2-} group and Bi^{3+} to Sm^{3+} ions. In addition, the optimal doping concentration of Sm^{3+} and Bi^{3+} are determined to be 4 and 8 mol%, respectively. The luminescence mechanism of Sm^{3+} singly doped sample and the energy transfer in Sm^{3+}/Bi^{3+} co-doped sample have also been discussed. Finally, $NaLa(MoO_4)_2$: 4 mol% Sm^{3+} $NaLa(MoO_4)_2$: 4 mol% Sm^{3+}, 8 mol% Bi^{3+} phosphors exhibit strong white emission and high efficiency. Their CIE chromaticity coordinates are both located in the white region; the maximum absolute quantum efficiencies is up to 52% under 405 nm excitation.

Acknowledgements

We would like to acknowledge the financial support received from the Science and Technology Foundation of Shenzhen, Shenzhen Science and Technology Innovation Committee (Grant No. JCYJ20160331173823401) and National Science Foundation of China (51372138).

References

[1] Benoît G, Véronique J, Arnaud A and Alain G 2011 *Solid State Sci.* **13** 460
[2] Kaczmarek A M and Deun R V 2013 *Chem. Soc. Rev.* **42** 8835
[3] Li L F, Dong D B, Zhang J Y, Zhang C M and Jia G 2014 *Mater. Lett.* **131** 298
[4] Mazzocchia C, Aboumrad C, Diagne C, Tempesti E, Herrmann J M and Thomas G 1991 *Catal. Lett.* **10** 181
[5] Spassky D, Ivanov S, Kitaeva I, Kolobanov V, Mikhailin V, Ivleva L *et al* 2005 *Phys. Status Solidi C* **2** 65
[6] Kim S S, Ogura S, Ikuta H, Uchimoto Y and Wakihara M 2001 *Chem. Lett.* **30** 760

[7] Sundaram R and Nagaraja K S 2004 *Sens. Actuators B: Chem.* **101** 353
[8] Zhou Y and Yan B 2013 *CrystEngComm.* **15** 5694
[9] Volkov V, Cascales C, Kling A and Zaldo C 2005 *Chem. Mater.* **17** 291
[10] Xue L P, Wang Y J, Lv P W, Chen D G, Lin Z, Liang J K *et al* 2009 *Crystal Growth Design* **9** 914
[11] Xu L, Yang X Y, Zhai Z, Gu D X, Pang H and Hou W H 2012 *CrystEngComm.* **14** 7330
[12] Zhang J C, Wang X F, Zhang X H, Zhao X D, Liu X Y and Peng L P 2011 *Inorg. Chem. Commun.* **14** 1723
[13] Liao J, Zhou D, You H, Wen H, Zhou Q and Yang B 2013 *Optik* **124** 1362
[14] Xu L, Yang X, Zhai Z, Chao X, Zhang Z and Hou W 2011 *CrystEngComm.* **13** 4921
[15] Liu S S, Yang D P, Ma D K, Wang S, Tang T D and Huang S M, 2011 *Chem. Commun.* **47** 8013
[16] Yang M, You H, Jia Y, Qiao H, Guo N and Song Y 2011 *CrystEngComm.* **13** 4046
[17] Xu Z, Li C, Li G, Chai R, Peng C, Yang D *et al* 2010 *J. Phys. Chem. C* **114** 2573
[18] Neeraj S, Kijima N and Cheetham A K 2004 *Chem. Phys. Lett.* **387** 2
[19] Tao Y, Zhao G, Zhang W and Xia S 1997 *Mater. Res. Bull.* **32** 501
[20] Igarashi T, Ihara M, Kusunoki T, Ohno K, Isobe T and Senna M 2000 *Appl. Phys. Lett.* **76** 1549
[21] Deng Y, Yi S, Wang Y and Xian J 2014 *Opt. Mater.* **36** 1378
[22] Wan J, Wang Z, Chen X, Mu L and Qian Y 2005 *J. Cryst. Growth* **284** 538
[23] Lei F and Yan B 2009 *J. Am. Ceram. Soc.* **92** 1262
[24] Patra A, Friend C, Kapoor R and Prasad N 2002 *J. Phys. Chem. B* **106** 1909
[25] Pan Y, Zhang Q, Zhao C and Jiang Z 2007 *Solid State Commun.* **142** 24
[26] Pramanik S and Bhattacharya S C 2010 *Mater. Chem. Phys.* **121** 125
[27] Li Y, Wang G, Pan K, Qu Y, Liu S and Feng 2013 *Dalton Trans.* **42** 3366
[28] Liu J, Xu B, Song C, Luo H, Zou X, Han L *et al* 2012 *CrystEngComm.* **14** 2936
[29] Nakamura S, Mukai T and Senoh M 1994 *J. Appl. Phys.* **76** 8189
[30] Neeraj S, Kijima N and Cheetham A K 2004 *Chem. Phys. Lett.* **387** 2
[31] Sivakumar V and Varadaraju U V 2005 *J. Electrochem. Soc.* **152** 168
[32] Kasturi S and Sivakumar V 2017 *Mater. Chem. Front*. **1** 550
[33] Raju K V, Raju N, Sailaja S, Dhoble S J and Reddy B S 2013 *J. Lumin.* **134** 297
[34] Kimani M M and Kolis J W 2014 *J. Lumin*. **145** 492
[35] Xu B, Hao J, Guo Q, Wang J, Bai G, Fei B *et al* 2014 *J. Mater. Chem. C* **2** 2482
[36] Ju G, Hu Y, Chen L, Wang X, Mu Z, Wu H *et al* 2012 *J. Lumin.* **132** 1853
[37] Zhang X, Zhou G, Zhou J, Zhou H, Kong P, Yu Z *et al* 2014 *RSC Adv.* **4** 13680
[38] Wu J and Yan B 2010 *J. Am. Ceram. Soc*. **93** 2188
[39] Marques A P A, Tanska M T S, Longo E, Tanaka E R L and Rosa I L V 2011 *J. Fluoresc.* **21** 893
[40] Sun L, Qiu Y, Liu T, Zhang J Z, Dang S, Feng J *et al* 2013 *ACS Appl. Mater. Interfaces* **5** 9585
[41] Lunstroot K, Nockemann P, Van Hecke K, Van Meervelt L, Görller-Walrand C, Binnemans K *et al* 2009 *Inorg. Chem.* **48** 3018
[42] Cui Z, Ye R, Deng D, Hua Y, Zhao S, Jia G *et al* 2011 *J. Alloys Compd.* **509** 3553
[43] Brito H F, Malta O L, Felinto M C F C, Teotonio E E S, Menezes J F S, Silva C F B *et al* 2002 *J. Alloys Compd.* **344** 293
[44] Yu-Chun Li, Yen-Hwei Chang, Yu-Feng Lin and Yi-Jing Lin 2016 *Appl. Phys. Lett.* 2016 **89** 081110
[45] Poort S H M, Blokpoel W P and Blasse G 1995 *Chem. Mater.* **7** 1547
[46] Blasse G 1969 *Philips Res. Rep.* **24** 131
[47] Huang S H and Lou L R 1990 *Chin. J. Lumin.* **11** 1
[48] Yan B and Wu J H 2009 *Mater. Chem. Phys.* **116**
[49] Li Y, Xia Y, Liao S, Long Q, Zhao X and Dai S 2014 *Mater. Lett.* **123** 112
[50] Qiao X, Cheng Y, Qin L, Qin C, Cai P, Kim S *et al* 2014 *J. Alloys Compd.* **617** 946